Original Article

INR INTERVENTIONAL NEURORADIOLOGY

Interventional Neuroradiology
0(00) 1–11
© The Author(s) 2016
Reprints and permissions:
sagepub.co.uk/journalsPermissions.nav
DOI: 10.1177/1591019915622169
ine.sagepub.com

SAGE

Time density curve analysis for C-arm FDCT PBV imaging

Mudassar Kamran and James V Byrne

Abstract

Introduction: Parenchymal blood volume (PBV) estimation using C-arm flat detector computed tomography (FDCT) assumes a steady-state contrast concentration in cerebral vasculature for the scan duration. Using time density curve (TDC) analysis, we explored if the steady-state assumption is met for C-arm CT PBV scans, and how consistent the contrast-material dynamics in cerebral vasculature are across patients.

Methods: Thirty C-arm FDCT datasets of 26 patients with aneurysmal-SAH, acquired as part of a prospective study comparing C-arm CT PBV with MR-PWI, were analysed. TDCs were extracted from the 2D rotational projections. Goodness-of-fit of TDCs to a steady-state horizontal-line-model and the statistical similarity among the individual TDCs were tested. Influence of the differences in TDC characteristics on the agreement of resulting PBV measurements with MR-CBV was calculated.

Results: Despite identical scan parameters and contrast-injection-protocol, the individual TDCs were statistically non-identical ($p < 0.01$). Using Dunn's multiple comparisons test, of the total 435 individual comparisons among the 30 TDCs, 330 comparisons (62%) reached statistical significance for difference. All TDCs deviated significantly ($p < 0.01$) from the steady-state horizontal-line-model. PBV values of those datasets for which the TDCs showed largest deviations from the steady-state model demonstrated poor agreement and correlation with MR-CBV, compared with the PBV values of those datasets for which the TDCs were closer to steady-state.

Conclusion: For clinical C-arm CT PBV examinations, the administered contrast material does not reach the assumed 'ideal steady-state' for the duration of scan. Using a prolonged injection protocol, the degree to which the TDCs approximate the ideal steady-state influences the agreement of resulting PBV measurements with MR-CBV.

Keywords

Parenchymal blood volume, C-arm flat detector computed tomography, cerebral blood volume, time density curve, MR perfusion-weighted imaging

Received 27 September 2015; accepted 22 November 2015

Introduction

C-arm imaging systems have traditionally been used for high-contrast vessel imaging in the interventional suite.[1] However, with the introduction of flat detector technology, novel reconstruction algorithms, and implementation of specially designed protocols, these systems are now capable of generating whole-brain parenchymal blood volume (PBV) maps in addition to providing cross-sectional soft-tissue images of brain parenchyma.[2] Initial reports have compared C-arm flat detector computed tomography (C-arm FDCT or C-arm CT) PBV measurements with computed tomography (CT) perfusion (CTP)-derived cerebral blood volume (CBV) both in canines and humans.[3–6] For the calculation of C-arm CT PBV, the intravenously administered iodinated contrast material is assumed to have reached a steady-state concentration in the cerebral vasculature ($C_{tissue} = C_{artery} = C_{vein}$), which is maintained for the duration of scan.[2] Based on this assumption, the C-arm CT PBV is inferred to be equivalent to the CBV derived from dynamic perfusion imaging modalities such as CTP or magnetic resonance (MR) perfusion-weighted imaging (MR-PWI). In our previous work, we demonstrated that C-arm CT PBV is a composite parameter with combined blood flow (~60%) and blood volume (~40%) weightings.[7] A preferential blood flow weighting noted for clinical C-arm CT PBV studies could be related to temporal

Nuffield Department of Surgical Sciences, University of Oxford, UK

Corresponding author:
Mudassar Kamran, Nuffield Department of Surgical Sciences, University of Oxford, Room 6607, Level 6, John Radcliffe Hospital, Headington, Oxford, OX3 9DU, UK.
Email: m.kamran@oxon.org

changes in the concentration of intravenously administered contrast in the cerebral vasculature. To what extent the steady-state assumption is met for the clinical C-arm CT PBV scans has not been studied.

This study aimed to: (a) test the assumption that iodinated contrast material administered using a standard injection protocol as part of C-arm CT PBV scan reaches a steady-state concentration in cerebral vasculature for the duration of scan, (b) explore how consistent the dynamics of contrast material in cerebral vasculature are across patients by using time density curve (TDC) analysis of the raw C-arm FDCT projection data, and (c) investigate the influence of differences in TDC characteristics of the clinical C-arm CT PBV scans on the resulting PBV measurements and their agreement with MR-CBV.

Materials and methods

Thirty C-arm FDCT PBV protocol scans of 26 patients were analysed. The clinical and imaging data were acquired as part of a prospective study comparing C-arm CT PBV with MR-PWI, approved by the local research ethics committee. The study included adult patients aged over 18 years with documented aneurysmal subarachnoid haemorrhage (SAH) who subsequently developed symptoms and signs suggesting delayed cerebral ischemia (DCI) and requiring confirmatory imaging – a situation necessitating admission and management in the neuro-intensive care unit (neuro-ICU). The diagnosis of DCI was based on clinical assessment by the multidisciplinary neuro-ICU team and was defined as clinical deterioration (focal neurological deficits or reduced level of consciousness) lasting two hours or longer with no evidence of rebleed or hydrocephalus on noncontrast CT (NCCT) head, and no other medical causes such as infections or metabolic disturbances to explain the clinical/neurological deterioration.

Exclusion criteria were: a history of allergy to iodinated contrast medium, renal impairment, pregnancy, or contraindications to MR examination. All recruited patients had undergone aneurysm repair by endovascular coil embolisation. Written informed consents were obtained from patients or, if they were unable to complete the consent process, from a family member or a designated surrogate as defined by the research ethics committee approval for the study. All recruited patients underwent an MR imaging (MRI) examination using a standard protocol that included diffusion- and perfusion-weighted sequences concurrent with a research C-arm CT scan using a PBV protocol. For all recruited individuals, we recorded age, gender, clinical status on admission (World Federation of Neurological Societies (WFNS) grade), amount of blood on the admission scan (Fischer grade), aneurysm location, and treatment. The imaging protocols and post-processing steps for C-arm FDCT and MR examinations are described in the following sections.

C-arm FDCT imaging

C-arm FDCT scan was performed on a flat detector equipped biplane angiography system (Axiom Artis dBA; Siemens Healthcare, Germany) in the neuro-interventional suite. The imaging protocol included two rotational acquisitions: mask and contrast-enhanced (or fill) runs. Projection data for each run were acquired using the following parameters: 419 projection images, 0.5-degree frame angle, 210-degree angular scan range, 8 seconds acquisition time, 0.36 μGy radiation dose per frame. The contrast-enhanced dataset was acquired following a manually triggered intravenous injection of radiographic contrast material, Niopam 370 (Bracco spa, Milan, Italy), using a power injector (Medrad Inc, Philadelphia, PA, USA). The injection parameters were: contrast concentration, 370 mg iodine/ml; volume, 80 ml; injection rate, 4 ml/sec through the antecubital vein; injection pressure, 300 pounds per square inch (psi); and injection duration, 20 seconds. Passage of contrast material through the cerebral vasculature was monitored on two-dimensional (2D) fluoroscopic images (two frames/second) and the contrast-enhanced run was triggered when maximal opacification of the superior sagittal sinus was observed.

Post-processing of the data to generate color-coded PBV maps was performed on a dedicated research workstation (Leonardo, Siemens AG, Healthcare) using prototype software (syngo Neuro PBV IR; Siemens Healthcare, Germany). The final PBV values were expressed in units of ml/100 gm of cerebral tissue.

MRI

A standard MR scan protocol comprising axial and sagittal T1-weighted, axial T2-weighted, diffusion-weighted, perfusion-weighted, and time-of-flight (TOF) angiography sequences was performed on a Philips Achieva 1.5 Tesla MRI unit. Perfusion data were acquired using the dynamic susceptibility contrast (DSC) technique with the following parameters: T2*-weighted gradient-echo echo planar sequence, repetition time (TR) 2000 ms, echo time (TE) 44 ms, field of view (FOV) 248×248 mm, reconstruction matrix 256×256, voxel size $0.98 \times 0.98 \times 4$ mm, sensitivity encoding (SENSE) factor 2.1, bandwidth 806 Hz/pixel, sequence duration 1 minute, 46 second. Paramagnetic contrast material was administered intravenously with an MR-compatible power injector (Medrad Inc) at 5 ml/sec followed by a 10 ml saline flush. Fifteen slices covering the whole brain were acquired at 50 time points following the injection of 0.2 mmol/kg of Gadopentate (Prohance, Bracco Diagnostics Inc, Italy)

Post-processing of the perfusion data was performed using a commercially available software (nordicICE perfusion package, NordicNeuroLab, Bergen, Norway), both Conformité Européenne (CE) marked

and United States (US) Food and Drug Administration (FDA) approved. After motion correction of the raw data, perfusion maps were created using the standard singular value deconvolution (SVD) technique. Arterial input function (AIF) to deconvolve the dynamic tissue response curve was automatically determined and SVD regularization was achieved with the truncated SVD approach (cut-off fraction 0.20) and iterative thresholding (target oscillation index 0.10). Semi-quantitative, leakage-corrected output perfusion maps for clinical interpretation included: cerebral blood flow (CBF), CBV, mean transit time (MTT), and time to peak (TTP).

Time density curve (TDC) analysis

Thirty C-arm FDCT datasets (26 patients), each comprising a mask and a contrast-enhanced (fill) run, were included in the analysis. The mask and the fill runs each consisted of 419 two-dimensional (2D) rotational projections, acquired over an angular scan range of 210 degrees and a time period of 8 seconds (two projections/degree; 52 projections/second). Rectangular regions of interest (ROIs) were applied to the 2D projections of mask and fill runs as depicted in Figure 1. To illustrate, on the mask run, a rectangular ROI was drawn on the first of 419 projections above the level of orbital roof and propagated to the remaining projections such that the ROI spanned the anterioposterior dimension of the head on the lateral projections and the lateral (coronal) dimension of the head on the frontal projections. Mean image intensity (IE) in the ROI for each projection of the mask run was measured (419 measurements). The same ROIs used for the mask run were subsequently applied to the co-registered projections of contrast-enhanced (fill) run and mean IEs in the ROIs of the fill run were measured (419 measurements). Mean IEs of the ROIs for the mask run projections were then subtracted from the mean IEs of the corresponding ROIs for the fill run projections. IE differences between the mask and the fill runs represented differences in the degree of x-ray attenuation between the two runs. The IE differences thus calculated for the rotational projections were corrected for sequential differences in the head diameter over the semi-circular scan trajectory by normalisation with the head thickness that the respective x-ray beam had to traverse. The corrected IE differences were related to the presence of iodinated contrast in cerebral vasculature administered intravenously as part of C-arm CT PBV protocol. These corrected IE differences between the mask and the fill runs for each patient were plotted against the number of projections (or time; frame rate 52 projections/sec) to generate TDCs. The TDC image analysis was performed using Image J software (Image J, US National Institutes of Health, Bethesda, MD, USA).

Quantitative VOI analysis

MR-CBV and C-arm CT PBV parametric maps were further post-processed using the FMRIB software library (FSL) tools.[8] The brain extraction tool (BET) was used to delete the non-brain tissues from the images of interest.[9] Linear registration of the C-arm PBV maps and the MR CBV maps for each patient was performed to the T1-weighted average structural template brain volume in the MNI152 space with the FMRIB linear image registration tool (FLIRT).[10] Binarised predefined cortical and subcortical volumes of interest (VOIs; 56 for each hemisphere encompassing the whole brain), as defined in the Harvard-Oxford structural brain atlas, were applied to the co-registered parametric maps. Mean, median and standard deviation values of each parameter were extracted for all VOIs encompassing both hemispheres. Inter-hemispheric ratios of each parameter were calculated (e.g. right PBV/left PBV = relative PBV or rPBV) and subsequently used for statistical analysis. Figure 2 provides an overview of these image post-processing steps.

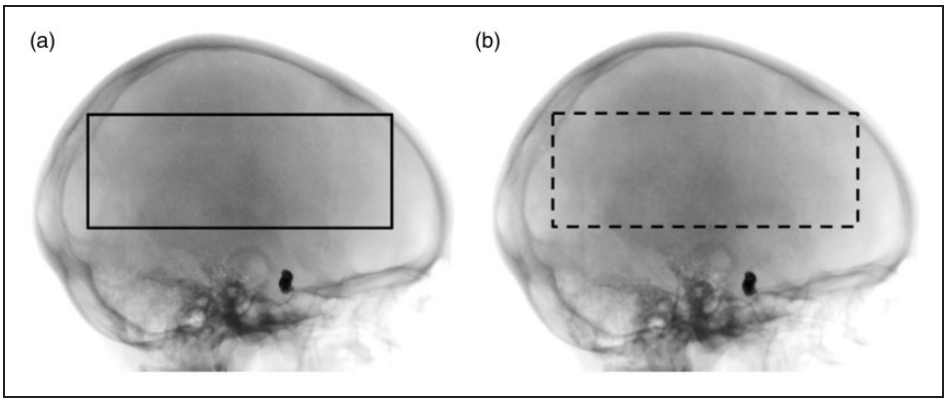

Figure 1. Illustration of ROI placement on the 2D C-arm FDCT rotational projections.
The rectangular ROIs were placed on the 2D projections of the mask run (a) and were subsequently transposed onto the respective projection of contrast-enhanced run (b). The IEs for rotational projections were then corrected for differences in the head diameter among the rotational projections. ROI: region of interest; 2D: two-dimensional; FDCT: flat detector computed tomography; IEs: image intensities.

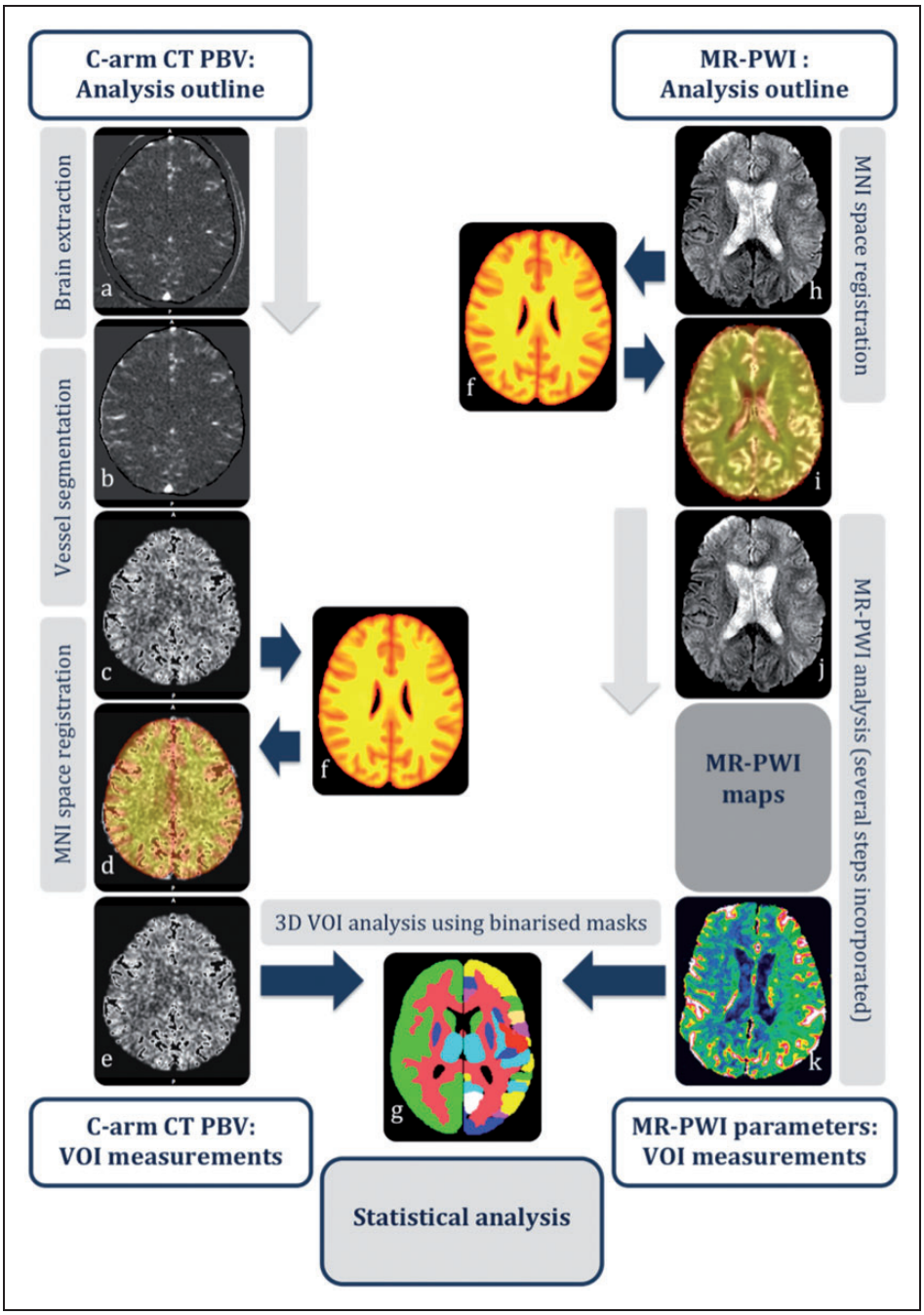

Figure 2. A schematic overview of the image post-processing for the VOI analysis.
(a) A C-arm CT PBV dataset before brain extraction; (b) PBV dataset following brain-extraction using FSL BET utility; (c) PBV dataset following threshold-based segmentation of the vascular structures; (d) registration of the PBV volume to the T1-weighted average structural template brain volume in MNI152 space; (e) brain-extracted, co-registered, vessel-segmented PBV volume in MNI152 space; (f) T1-weighted average structural template brain volume in MNI152 space to which the C-arm CT PBV maps and the MR-PWI data were coregistered; (g) binarised 3D-VOIs of cortical and subcortical structures encompassing the whole brain; (h) dynamic T2*-weighted MR-PWI dataset; (i) registration of the MR-PWI to T1-weighted average structural template brain volume in MNI152 space; (j) registered MR-PWI dataset which was subsequently post-processed to extract perfusion parametric maps preserving the spatial coordinates in MNI152 space; (h) motion-corrected, vessel-segmented, brain-extracted, leakage-corrected, registered MR-PWI maps. Subsequently, using the binarised 3D-VOIs, the perfusion parametric values were obtained for the cortical and subcortical structures, which were then used in the statistical analysis. VOI: volume of interest; CT PBV: computed tomography parenchymal blood volume; FSL: FMRIB software library; BET: brain extraction tool; MR-PWI: magnetic resonance perfusion-weighted imaging; 3D: three-dimensional.

Statistical analysis

Gross patterns of the TDCs were initially explored using a model-free curve-fitting methodology. Locally weighted-scatterplot-smoothing (LOWESS) was applied to the scatterplots of IE differences vs time to generate smooth TDCs (a model-free curve-fitting approach that uses local weights for TDC smoothing was chosen to preserve the measured characteristics of the curves). D'Agostino-Pearson normality test was performed to evaluate if the data followed a Gaussian distribution. IE differences were noted to deviate significantly from the normal distribution prompting non-parametric statistical analysis.

To explore if the TDCs for individual datasets met the steady-state assumption, a horizontal line model computed for each dataset using the least-squares method was employed which represented the ideal steady-state contrast material concentration in the cerebral vasculature. Nonlinear regression analysis was used to fit the steady-state horizontal line model to each TDC dataset. Parameters for goodness-of-fit to the steady-state model were calculated and Runs test was performed to evaluate if there was significant deviation of the data points on the measured TDCs from the steady-state model.

To test the statistical similarity among the TDCs for individual C-arm CT datasets, we employed non-parametric Kruskal-Wallis test. Dunn's multiple comparisons test was subsequently performed to compare each dataset's TDC to every other dataset's TDC and the p-values adjusted for multiple comparisons were computed.

In the next step, to test if the differences in temporal characteristics of the TDCs contribute toward differences in final PBV measurements and their agreement with MR-CBV, the C-arm CT PBV datasets were segregated into two groups. Group A included 10 datasets for which the TDCs showed the largest deviations from the horizontal line steady-state model (Figure 3; datasets 21–30) while group B included 20 datasets for which the TDCs were closer to steady-state (Figure 3; datasets 1–20). For the two groups, Pearson correlation and Bland-Altman analysis were performed to explore the correlation and agreement of the C-arm CT rPBV values with the MR-rCBV for cortical and subcortical VOIs. All statistical analysis was performed using GraphPad Prism version 6.0a (GraphPad Software, San Diego CA, USA).

Results

Patient characteristics

Thirty C-arm FDCT datasets of 26 patients (mean age 55 years; nine men, 17 women) acquired using PBV protocol were reviewed. All patients had aneurysmal SAH on admission and underwent coil embolisation. On the admission NCCT head, the SAH Fischer grades were: Grade 4 in 16 (61%), Grade 3 in nine (35%), while one patient's initial NCCT head did not show evidence of SAH which was proven on lumbar puncture (4%). WFNS grades at the time of initial presentation were: Grade 1 in 16 (61%), Grade 2 in seven (27%), Grade 3 in two (8%) and Grade 4 in one patient (4%). The patient characteristics are summarised in Table 1.

Statistical analysis

The LOWESS TDCs for each dataset illustrating the gross patterns of contrast material dynamics are depicted in Figures 3 and 4. A visual comparison of smoothed TDCs shows that while temporal characteristics of some TDCs depart markedly from the steady-state (Figure 3; datasets 21–30), a greater proportion of TDCs remain fairly closer to the expected steady-state with minimal slow upslope or downslope during the scan interval (Figure 3; datasets 1–20). Descriptive statistics for the differences in image intensity between the mask and the contrast-enhanced runs' projections measured over time are summarised in Table 2.

The initial results of Kruskal-Wallis test demonstrated that despite the identical scan parameters and contrast material injection protocols, the 30 TDCs are statistically non-identical (Kruskal-Wallis statistic 3722; $p < 0.0001$). Subsequent Dunn's multiple comparisons test showed that of the total 435 individual comparisons among the 30 TDCs, 330 comparisons (62%) reached statistical significance for difference (adjusted p-value < 0.0001) while the remaining 105 comparisons (38%) did not reach statistical significance for difference.

Horizontal line steady-state model fit to each dataset was performed as depicted in Figure 5. The runs test showed that all the TDCs deviated significantly ($p < 0.0001$) from the ideal steady-state horizontal line model constructed individually for each dataset.

The results of subgroup agreement and correlation analysis of C-arm CT rPBV vs MR-rCBV were: (a) Group A: bias 0.052 ± 0.31 and 0.065 ± 0.29; 95% limits of agreement -0.65 to 0.75 and -0.62 to 0.74; and Pearson correlation coefficient (r), 0.60 (95% confidence interval (CI): 0.55 to 0.64) and 0.58 (95% CI 0.54 to 0.63), for cortical and subcortical VOIs respectively; and (b) Group B: bias 0.026 ± 0.18 and 0.030 ± 0.18; 95% limits of agreement -0.24 to 0.29 and -0.27 to 0.33; and Pearson correlation coefficient (r), 0.84 (95% CI: 0.81 to 0.87) and 0.81 (95% CI 0.77 to 0.84), for cortical and subcortical VOIs, respectively. Thus the PBV values for the datasets with the largest deviations of TDCs from the horizontal line steady-state model had both poor agreement and worse correlation with MR CBV, compared with the PBV values for those datasets with TDCs closer to the steady-state.

Discussion

Our results demonstrate that despite the same scan parameters and identical contrast injection protocols, the

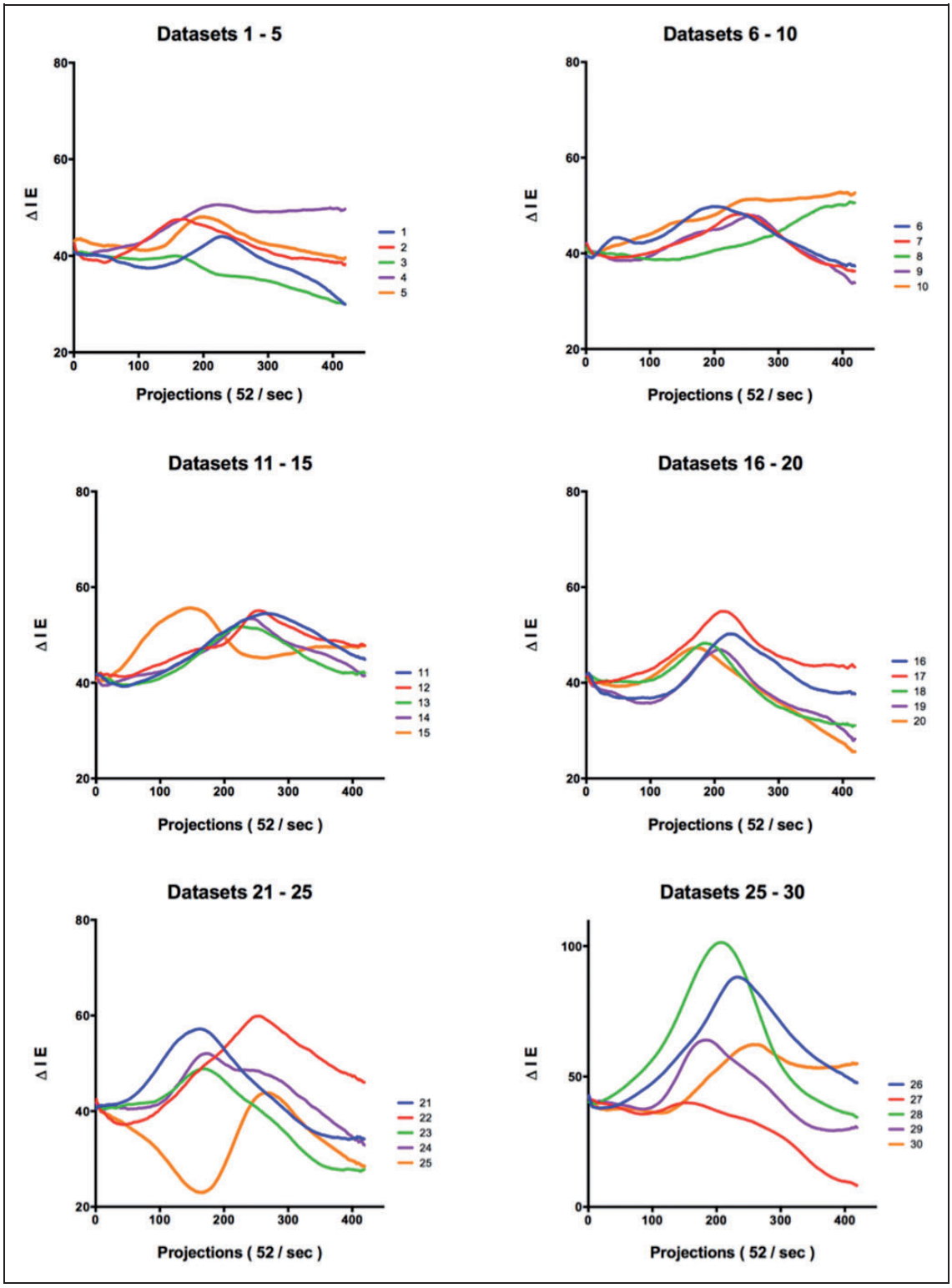

Figure 3. Locally weighted-scatterplot-smoothed (LOWESS) TDCs in subgroups.
TDCs for the datasets grouped according to the degree of approximation to steady-state, e.g. TDCs of datasets 1–5 show close approximation to ideal steady-state while TDCs for datasets 25–30 show marked deviation from steady state. TDCs: time density curves.

temporal characteristics of measured TDCs vary significantly among patients undergoing C-arm CT PBV examination. Furthermore, the administered contrast material does not reach the assumed 'ideal steady-state' in the cerebral vasculature for the duration of the scan. However, the TDC temporal characteristics of most datasets remain close to the steady-state while TDCs of some datasets deviate markedly from the steady-state. The degree to which the measured TDCs approximate the steady-state influences the agreement

Table 1. Demographic, aneurysm, and clinical characteristics of the study population.

Patient number	Age (years)	Gender (M/F)	Aneurysm location	Aneurysm size (mm)	WFNS grade	Fischer grade
1	47	M	Anterior communicating artery	6 × 4	1	3
2	55	F	Left anterior cerebral artery	12 × 10	3	4
3	61	F	Right posterior communicating artery	8 × 5	2	3
4	49	F	Anterior communicating artery	10 × 7	1	3
5	68	F	Right posterior communicating artery	10 × 6	2	4
6	71	F	Anterior communicating artery	6 × 5	1	4
7	46	M	Right middle cerebral artery	4 × 3	3	3
8	77	F	Left anterior cerebral artery	6 × 4	1	4
9	46	M	Right posterior communicating artery	4 × 4	1	4
10	50	F	Right internal carotid artery	3 × 3	1	3
11	53	F	Basilar artery tip	7 × 6	2	3
12	55	M	Right posterior communicating artery	5 × 3	2	4
13	55	F	Left posterior communicating artery	4 × 4	2	4
14	69	F	Left anterior cerebral artery	11 × 7	1	4
15	66	M	Anterior communicating artery	7 × 5	1	0[a]
16	45	M	Anterior communicating artery	15 × 8	2	4
17	66	M	Right middle cerebral artery	8 × 3	4	4
18	30	M	Anterior communicating artery	7 × 4	1	3
19	39	F	Right posterior communicating artery	5 × 3.5	1	4
20	50	F	Anterior communicating artery	4 × 3.5	1	4
21	69	M	Right posterior communicating artery	7 × 4	1	4
22	39	F	Right posterior communicating artery	10 × 9	1	4
23	52	F	Right posterior communicating artery	5 × 5	1	4
24	54	F	Left posterior communicating artery	8 × 5	1	3
25	58	F	Right anterior cerebral artery	5 × 4	1	3
26	60	F	Left peri-callosal artery	12 × 8	2	4

[a]NCCT head was negative for SAH, which was later confirmed on lumbar puncture.
M: male; F: female; NCCT: noncontrast computed tomography; SAH: subarachnoid haemorrhage; WFNS: World Federation of Neurological Societies.

of resulting PBV values with MR-CBV. This is illustrated by our findings that the rPBV values of those datasets for which the TDCs showed largest deviations from the steady-state model demonstrated poor agreement and correlation with MR-rCBV, compared with the rPBV values of those datasets for which the TDCs were closer to the steady-state.

Multiple factors may explain: (a) why a steady-state contrast concentration is not achieved in the cerebral vasculature despite a prolonged slow contrast injection (duration 20 sec, rate 4 ml/sec; the current standard for C-arm CT PBV imaging), and (b) why differences in temporal characteristics of TDCs exist among individuals despite identical contrast injection protocol and scan parameters. Given the identical injection and scan parameters, only patient factors can explain the observed differences. Regarding '(a)', from a physiological standpoint, following a peripheral intravenous contrast injection, bolus dispersion occurs that is governed by factors such as regional blood flow and tissue perfusion. For prolonged injections, recirculation of the contrast becomes an important factor. Normal recirculation times may range 15–40 seconds. Given the 20-second long injection that is used for C-arm CT PBV protocol, some recirculation of contrast would thus begin during the contrast material administration. The recirculated contrast-enhanced blood would reach the cerebral circulation in a non-simultaneous fashion due to multiple circulatory pathways in the body. Consequently, the new contrast medium and the recirculated contrast medium may mix and lead to a gradual increase in the concentration of contrast material in cerebral circulation. In addition, a power-injected large contrast volume accelerates the slow peripheral venous blood flow and may perturb the haemodynamic physiology of the cardiovascular system to a variable extent. This haemodynamic perturbation effect is more significant for a larger contrast volume, administered at a higher injection rate. As a result of recirculation and hemodynamic perturbation effect, the steady-state is not sustained and the TDC may show an upslope or downslope. In regards to '(b)', the between-subject differences in the TDCs may also be explained by multiple patient-related factors of which the most important are

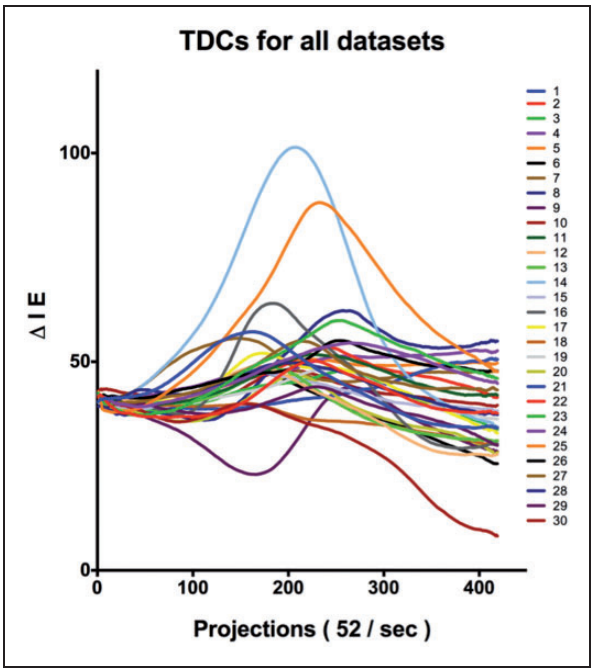

Figure 4. Locally weighted-scatterplot-smoothed (LOWESS) TDCs (aggregated).
The measured TDCs for C-arm FDCT datasets ($n = 30$) show that while the majority of the TDCs remain close to a steady-state (a steady-state TDC is expected to be a horizontal line with no upslope or downslope), some TDCs deviate markedly from the expected steady-state. TDCs: time density curves; FDCT: flat detector computed tomography.

differences in body size, i.e. height and weight, cardiovascular recirculation time (determined by cardiac output), age and gender.[11] Additionally, the cerebrovascular physiology may be altered to a variable extent in various patients following aneurysmal SAH due to factors such as vessel narrowing and microvascular dysfunction. Lastly, permeabilities at the microvasculature-cellular interface in the cerebral tissue become important if there has been breakdown of the blood-brain barrier (BBB), and can differ among patients, thereby contributing to the between-subjects differences.

Understanding the contrast material dynamics in cerebral vasculature is important when calculating and interpreting a perfusion parameter. The C-arm systems in current clinical use are limited in their temporal resolution due to slow rotational speed (minimum 5 seconds); the temporal resolution is further degraded by their inability to rotate continuously in the same direction.[12] Gantry rotation time for C-arm CT PBV scanning is typically 6–10 seconds, which is too long to adequately resolve voxel-wise TDCs and thus to apply the standard CTP algorithms.[2] As a result, only PBV measurements can be performed with the current C-arm systems using a specially designed prolonged injection protocol that aims to achieve steady-state contrast concentration in the entire cerebral vasculature. For a single compartment model using the dynamic perfusion imaging, the CBV can be calculated using equation 1:

$$\mathrm{CBV} = \frac{\int_0^\infty C_{tissue}(t)\mathrm{d}t}{\int_0^\infty C_{artery}(t)\mathrm{d}t} = \frac{\int_0^\infty C_{tissue}(t)\mathrm{d}t}{\int_0^\infty C_{vein}(t)\mathrm{d}t} \quad (1)$$

With an ideal steady-state contrast concentration achieved in cerebral vasculature ($C_{tissue} = C_{artery} = C_{vein}$), and no change in contrast concentration over the scan duration), equation 1 can be replaced by equation 2:

$$\mathrm{CBV} = \frac{C_{tissue}}{C_{artery}} = \frac{C_{tissue}}{C_{vein}} \quad (2)$$

The C-arm CT PBV measurements performed using the steady-state imaging would thus be equivalent to the CBV derived from dynamic perfusion imaging.[2,13] However, if the steady-state were not achieved, as is shown by the temporal shape of the TDCs in Figures 3 and 4, the resulting PBV measurements would not be equivalent to CBV and could only have a certain blood-volume weighting. Given the iodinated contrast material used for x-ray imaging consists of relatively small molecules that are highly diffusible, delivery of contrast material through the circulation to a tissue of interest is primarily flow limited.[11] Thus an upslope or downslope of the TDC would indicate preferential contrast wash-in or wash-out into the tissue of interest and could impart a blood-flow weighting to the PBV measurements, which explains our previously reported observations documenting a ~60% blood-flow and ~40% blood-volume weighting to PBV measurements.[7] The greater the TDC deviates from the ideal steady-state, the lesser would be the equivalence of C-arm CT PBV to CBV. The above discussion explains the results of subgroup analysis where the PBV values of those datasets for which the TDCs showed largest deviations from the steady-state model also demonstrated poor agreement and correlation with MR-CBV, compared with the PBV values of those datasets for which the TDCs were closer to the steady-state. These issues have previously not been explored for C-arm CT PBV imaging. However, our results are supported by observations for MD-CTA where: (a) a slow contrast injection, long injection-to-scan delay, and longer scanning facilitate blood-volume weighting,[14] (b) higher contrast injection rates (5–7 ml/sec), shorter injection-to-scan delay, and faster scanning alter the temporal shape of TDC and eliminate the near steady-state during acquisition of CTA images. Consequently the resulting computed tomography angiography (CTA) source images (and MDCT PBV images) are less blood-volume weighted and more blood-flow weighted, similar to our findings for C-arm CT PBV.[15,16]

Abnormalities identified on the CBV and CBF maps (from dynamic perfusion imaging modalities) are known to represent different underlying tissue injury

Table 2. TDC descriptive statistics for the differences in image intensity between the mask and the contrast-enhanced runs' projections measured over time.

Dataset	Projections	Mean	SD	SEM	IQR	Minimum	Maximum	Skewness	Kurtosis
1	419	44.64	9.28	0.45	13.13	27.14	64.55	0.48	−0.75
2	419	41.19	6.70	0.33	8.46	27.31	61.09	0.84	0.23
3	419	48.43	9.27	0.45	13.62	29.69	69.97	0.05	−0.65
4	419	47.31	6.39	0.31	11.07	33.58	61.82	−0.07	−1.04
5	419	60.75	19.18	0.94	25.32	32.95	109.5	0.71	−0.34
6	419	47.64	5.90	0.29	6.85	34.49	67.04	0.79	0.85
7	419	45.86	6.43	0.31	7.23	32.87	63.46	0.87	0.28
8	419	44.19	4.97	0.24	7.99	31.17	55.6	0.13	−0.69
9	419	38.90	4.14	0.20	5.05	27.31	51.54	0.30	0.50
10	419	30.71	10.87	0.53	12.34	4.369	46.65	−1.00	−0.02
11	419	44.83	5.84	0.29	9.03	29.89	58.73	0.29	−0.71
12	419	39.16	8.17	0.40	10.80	20.27	55.98	−0.21	−0.69
13	419	39.24	6.91	0.34	9.55	25.01	58.19	0.38	−0.41
14	419	61.98	27.12	1.33	43.48	32.08	121	0.78	−0.83
15	419	42.09	4.65	0.23	6.05	32.35	59.07	0.45	0.01
16	419	43.50	14.66	0.72	14.88	20.96	82.58	0.99	0.31
17	419	44.00	6.97	0.34	8.91	27.35	62.83	0.52	0.04
18	419	36.71	3.72	0.18	6.41	27.05	44.92	−0.26	−0.79
19	419	41.98	4.77	0.23	6.57	31.42	53.69	0.40	−0.56
20	419	38.11	6.43	0.31	8.00	22.92	54.5	0.71	0.00
21	419	42.59	5.09	0.25	6.91	31.2	57.4	0.54	−0.05
22	419	46.05	5.34	0.26	6.24	35.16	63.29	0.81	0.58
23	419	41.76	5.06	0.25	7.65	30.01	54.57	0.29	−0.56
24	419	47.94	4.69	0.23	7.04	36.49	59.03	−0.28	−0.71
25	419	46.91	4.41	0.22	6.83	36.9	55.85	−0.37	−0.85
26	419	38.86	6.69	0.33	8.35	22.83	54.32	−0.02	−0.40
27	419	48.39	5.93	0.29	9.16	36.61	62.17	0.41	−0.85
28	419	48.45	11.49	0.56	18.23	27.42	77.75	0.24	−0.86
29	419	33.98	9.36	0.46	12.00	14.32	54.61	0.15	−0.56
30	419	42.97	4.06	0.20	4.80	35.47	55.69	0.88	0.33

IQR: interquartile range.

and each has a unique prognostic significance. Therefore, in a clinical setting, it is important to know how well the steady-state assumption was met for a particular PBV study and if the measured C-arm CT PBV is predominately blood-volume or blood-flow weighted. Diminished CBF with relatively preserved CBV indicates ischaemia, i.e. salvageable tissue (ischemic penumbra in stroke patients); whereas decreased CBV (and therefore decreased CBF) indicates infarction i.e. non-salvageable tissue (infarct core in stroke patients).[17] In a neuro-interventional setting, the distinction between the two has important implications for patient management. To illustrate this, consider a procedural setting where an ischemic stroke patient is undergoing revascularisation treatment, and the operator performs a C-arm CT PBV scan to assess the brain viability and to guide the treatment planning. In this situation if there is significant enlargement of the pre-treatment PBV abnormality or development of new large PBV abnormality: An equivalence of PBV to CBV (steady-state achieved) would indicate tissue infarction favouring treatment termination; on the contrary, a significant blood-flow weighting to PBV (steady-state not achieved) may indicate only ongoing tissue ischaemia and thus further revascularisation attempts may be beneficial.

We propose that a simple ROI-based TDC analysis of the raw C-arm CT projection data be implemented in the workflow of PBV scanning. It would provide an estimate of how adequately the steady-state contrast concentration was achieved during a particular C-arm CT PBV scan, which would inform the clinician interpreting the PBV maps on how closely an abnormality detected on PBV maps might correlate to a CBV (surrogate for infarction) or a CBF (surrogate for ischemia) abnormality. Assuming a steady-state in all patients may overlook the blood-flow weighting to C-arm CT PBV in cases where the TDCs depart significantly from

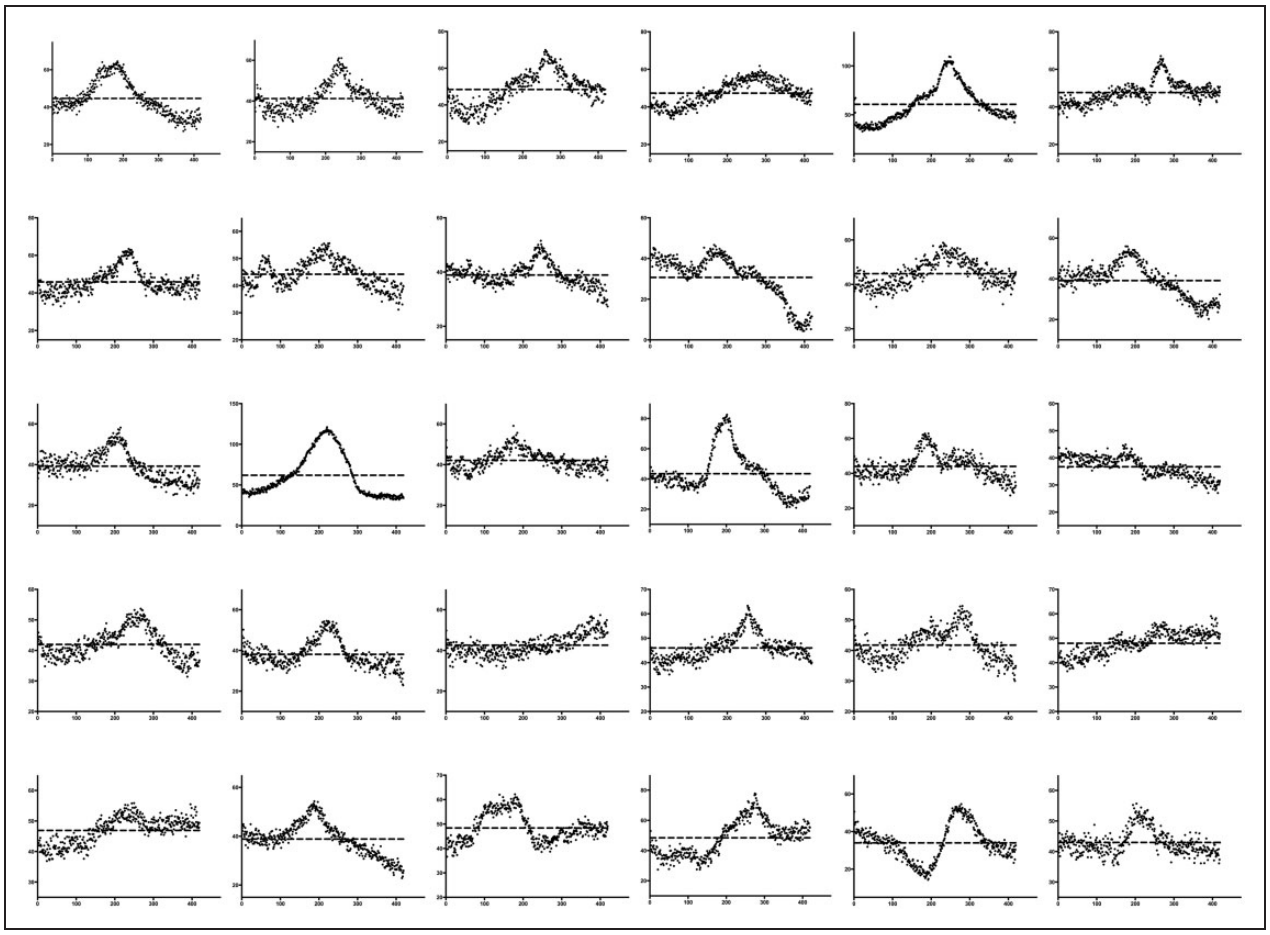

Figure 5. Steady-state model fitting for the TDCs.
Plots of horizontal line steady-state model fit for TDCs ($n = 30$) using nonlinear regression analysis. TDCs: time density curves.

the steady-state, thus potentially resulting in under-estimation of salvageable brain tissue.

Conclusion

This study demonstrates that for clinical C-arm CT PBV examinations, the administered contrast material does not reach the assumed 'ideal steady-state' for the duration of the scan, and the temporal characteristics of TDCs vary significantly among patients despite the same scan parameters and identical contrast material injection protocol. However, using a consistent prolonged injection protocol, TDCs for most datasets approximate the assumed steady-state. The degree to which this approximation is achieved influences the blood-volume weighting and the agreement of resulting PBV measurements with CBV. These factors have not been studied previously for the clinical C-arm CT PBV scans and are of clinical significance; for example, a knowledge of how adequately the steady-state was achieved during a PBV scan can inform the clinician interpreting the PBV maps on how closely the abnormality detected on PBV maps might correlate to a CBV or a CBF abnormality, each of which represents different underlying tissue injury and have unique prognostic significance. Assuming a steady-state in all patients may over-estimate blood-volume weighting to C-arm CT PBV in cases where the TDCs depart significantly from the steady-state, thus potentially resulting in under-estimation of salvageable brain tissue.

Acknowledgements

Author contributions include: M Kamran: project development, data collection and analysis, manuscript writing; and JV Byrne: project design, data collection, manuscript review.

We declare that all human and animal studies have been approved by the Coventry Research Ethics Committee and have therefore been performed in accordance with the ethical standards laid down in the 1964 Declaration of Helsinki and its later amendments. We declare that all patients gave informed consent prior to inclusion in this study.

We thank Siemens for hardware and software support. We are grateful to the members and staff of the Neuroradiology Department, John Radcliffe Hospital, Oxford, where all the imaging data were acquired for this study.

Funding

The authors disclosed receipt of the following financial support for the research, authorship, and/or publication of

this article: A small one-off grant to support work indirectly related to the project reported in this article was made by Siemens to the University of Oxford, UK.

Declaration of conflicting interests

The authors declared no potential conflicts of interest with respect to the research, authorship, and/or publication of this article.

References

1. Kamran M, Nagaraja S and Byrne JV. C-arm flat detector computed tomography: The technique and its applications in interventional neuro-radiology. *Neuroradiology* 2010; 52: 319–327.
2. Zellerhoff M, Deuerling-Zheng Y, Strother CM, et al. Measurement of cerebral blood volume using angiographic C-arm systems. *Biomedical Applications in Molecular, Structural, and Functional Imaging* 2009; 7262: 72620H.
3. Ahmed AS, Zellerhoff M, Strother CM, et al. C-arm CT measurement of cerebral blood volume: An experimental study in canines. *Am J Neuroradiol* 2009; 30: 917–922.
4. Bley T, Strother CM, Pulfer K, et al. C-arm CT measurement of cerebral blood volume in ischemic stroke: An experimental study in canines. *AJNR Am J Neuroradiol* 2010; 31: 536–540.
5. Struffert T, Deuerling-Zheng Y, Kloska S, et al. Flat detector CT in the evaluation of brain parenchyma, intracranial vasculature, and cerebral blood volume: A pilot study in patients with acute symptoms of cerebral ischemia. *Am J Neuroradiol* 2010; 31: 1462–1469.
6. Struffert T, Deuerling-Zheng Y, Kloska S, et al. Cerebral blood volume imaging by flat detector computed tomography in comparison to conventional multislice perfusion CT. *Eur Radiol* 2011; 21: 882–889.
7. Kamran M and Byrne JV. C-arm flat detector computed tomography parenchymal blood volume imaging: The nature of parenchymal blood volume parameter and the feasibility of parenchymal blood volume imaging in aneurysmal subarachnoid haemorrhage patients. *Neuroradiology* 2015; 57: 937–949.
8. Jenkinson M, Beckmann CF, Behrens TEJ, et al. FSL. *Neuroimage* 2012; 62: 782–790.
9. Smith SM. Fast robust automated brain extraction. *Hum Brain Mapp* 2002; 17: 143–155.
10. Jenkinson M, Bannister P, Brady M, et al. Improved optimization for the robust and accurate linear registration and motion correction of brain images. *Neuroimage* 2002; 17: 825–841.
11. Bae KT. Intravenous contrast medium administration and scan timing at CT: Considerations and approaches. *Radiology* 2010; 256: 32–61.
12. Fieselmann A, Ganguly A, Deuerling-Zheng Y, et al. Interventional 4-D C-arm CT perfusion imaging using interleaved scanning and partial reconstruction interpolation. *IEEE Trans Med Imaging* 2012; 31: 892–906.
13. Hamberg LM, Hunter GJ, Kierstead D, et al. Measurement of cerebral blood volume with subtraction three-dimensional functional CT. *Am J Neuroradiol* 1996; 17: 1861–1869.
14. Hunter GJ, Hamberg LM, Ponzo JA, et al. Assessment of cerebral perfusion and arterial anatomy in hyperacute stroke with three-dimensional functional CT: Early clinical results. *Am J Neuroradiol* 1998; 19: 29–37.
15. Konstas AA, Goldmakher GV, Lee TY, et al. Theoretic basis and technical implementations of CT perfusion in acute ischemic stroke, Part 1: Theoretic basis. *Am J Neuroradiol* 2009; 30: 662–668.
16. Sharma M, Fox AJ, Symons S, et al. CT angiographic source images: Flow- or volume-weighted? *Am J Neuroradiol* 2011; 32: 359–364.
17. Allmendinger AM, Tang ER, Lui YW, et al. Imaging of stroke: Part 1, perfusion CT—overview of imaging technique, interpretation pearls, and common pitfalls. *AJR Am J Roentgenol* 2012; 198: 52–62.